J Mater Sci (2015) 50:4174–4186
DOI 10.1007/s10853-015-8933-0

Hierarchically decorated electrospun poly(ε-caprolactone)/nanohydroxyapatite composite nanofibers for bone tissue engineering

Xin Jing · Elizabeth Jin · Hao-Yang Mi · Wan-Ju Li · Xiang-Fang Peng · Lih-Sheng Turng

Received: 19 September 2014 / Accepted: 25 February 2015 / Published online: 7 April 2015

Abstract Bone is a nanocomposite comprised of two main components, nanohydroxyapatite (nHA) and Type I collagen. The aim of this study is to mimic the nanotopography of collagen fibrils in bone tissue and to modulate their cellular functions by nanoscale stimulation. Three-dimensional structures consisting of electrospun poly(ε-caprolactone) (PCL) and PCL/nHA composite nanofibers decorated by periodically spaced PCL crystal lamellae (shish–kebab structure) were created. It was found that the hierarchically decorated nanostructure not only enhanced the mechanical properties of the scaffolds but also changed the surface wettability behavior of the scaffolds. The enhanced surface wettability facilitated biomimetic mineralization through apatite deposition when exposed to simulated body fluids (SBF). MG-63, an osteosarcoma cell line which behaves similarly to osteoblasts, was used to study the cellular response to the scaffolds. Data suggest kebab crystal nanotopography facilitating cell attachment and proliferation. Functional assays, which quantify alkaline phosphatase (ALP) and calcium expression, revealed increased ALP activity and increased calcium expression on decorated nanofibers. In addition, compared with other scaffolds, the cells on PCL/nHA nanofibrous shish–kebab-structured scaffolds showed obvious extended pseudopodia of the filaments in the cytoskeleton study, demonstrating better interactions between cells and scaffolds.

Introduction

Bone acts as a scaffold to give shape, structure, and strength to the frame of humans and animals. Starting from the macroscopic structural level, bone at different anatomical locations is diverse in shape and size due to the wide variety of their respective functions. However, although they have different macrostructures, the nanostructure comprised collagen fibrils embedded within organized hydroxyapatite (HA) crystals is the feature that they have in common [1]. The HA-collagen fibrils are about 100 nm in diameter and have a unique banding pattern with a period of 67 nm, which can be attributed to the periodically distributed HA crystals within the gap zones of the collagen fibrils [2]. HA crystals are produced by osteoblasts and resemble flat plates arranged parallel to one another on the long axis of the collagen fibrils [3]. Attempts to mimic the mineralized behavior in bone tissue have used a variety of materials such as gelatin [4], polylactic acid [5], and polycaprolactone [6], and composites [7]. Altering scaffold architecture by changing pore size [8] or fiber alignment [9] has also been used in an attempt to mimic bone mineralization. However, in spite of extensive research on biomimetic behaviors, no synthetic template has been proposed to mimic collagen fibrils with controlled mineral growth and orientation for bone tissue engineering.

X. Jing · H.-Y. Mi · X.-F. Peng (✉)
The Key Laboratory for Polymer Processing Engineering of Ministry of Education, National Engineering Research Center of Novel Equipment for Polymer Processing, South China University of Technology, Guangzhou, Guangdong, China
e-mail: pmxfpeng@scut.edu.cn

E. Jin · W.-J. Li
Departments of Orthopedics and Rehabilitation, and Biomedical Engineering, University of Wisconsin–Madison, Madison, WI, USA

L.-S. Turng (✉)
Wisconsin Institutes for Discovery, University of Wisconsin–Madison, Madison, WI, USA
e-mail: turng@engr.wisc.edu

Electrospun nanofibers have been widely used as tissue engineering scaffolds because nanofiber architecture resembles the structure of the natural extracellular matrix (ECM) [10]. Recently, particular attention has been devoted to fabricating composites of electrospun scaffolds containing organic polymers and inorganic salts, especially the PCL/HA system. It has been found that the addition of HA not only enhances the tensile strength of PCL scaffolds [11] but also acts as a chelating agent to accelerate the mineralization of human fetal osteoblast cells to form bone-like apatite for bone tissue engineering [12]. Puppi et al. prepared PCL nanofibrous scaffolds embedded with bisphosphonate and HA by electrospinning and wet-spinning and characterized various experimental parameters on the morphologies of the resultant fibers [13]. Recently, it was reported that the solvent used [methylene chloride and combined solvent methylene chloride and dimethylformamide (DMF)] in preparing the electrospun PCL/HA composite mats resulted in different bioactivities of the scaffolds, further affecting human mesenchymal stem cell (hMSC) proliferation and differentiation on the scaffolds. The authors found that using methylene chloride as the solvent led to larger pore sizes in the PCL/HA composite scaffolds, which were better for cell filtration in their study [14]. However, man-made nanofibers possess a smooth surface unlike the periodic nanostructure topography featured on the surface of natural collagen nanofibrils in ECM [15]. Since the topography that cells experience during cell–ECM interactions could affect the cell shape, mobility, proliferation, and differentiation [16], it is desirable to produce a structure showing a similar nanotopography to that of natural collagen fibrils.

The shish–kebab morphology was first observed in the extensional flow of polymer melts [17] and in polymer solutions [18] in the mid-1960s. The stretched polymer chains, shish, are surrounded by folded chain lamellae, kebabs, which periodically attached along the shish. In 2005, Li et al. successfully synthesized a novel nanohybrid shish–kebab (NHSK) by growing polyethylene and polyamide (Nylon) 6, 6 on carbon nanotubes via solution crystallization. He proposed "size-dependent soft epitaxy" to explain the NHSK formation mechanism [19].

Inspired by the formation of NHSKs, Chen et al. successfully mimicked the hierarchical structure of natural bone by facilitating PCL-b-poly(acrylic acid) (PCL-b-PAA) block copolymer self-assembly and one-dimensional polymer nucleation processes on PCL nanofibers [20]. In this structure, instead of using carbon nanotube as shish in NHSK, electrospun nanofibers were employed as shish to fabricate the shish–kebab structure. In our lab, we also tried to use a PCL shish–kebab structure, which consisted of PCL electrospun nanofibers as shish and periodic-spaced PCL crystal lamellae as kebabs, to mimic collagen fibrils. The 3T3 fibroblast cell culture results suggested that the nanotopography of the nanofiber surface with kebab crystals that mimicked collagen fibrils facilitated cell attachment and spreading [21]. Hence, one of the goals of this study was to investigate the potential applications of this special structure in bone tissue engineering.

This study aims to fabricate a nanofiber shish–kebab structure (NFSK) by using PCL/nHA composite nanofibers as the shish to be decorated by periodically spaced PCL lamella crystals (kebabs) to combine the advantage of the good compatibility of HA and the enhanced surface roughness introduced by the shish–kebab structure. The influence of the shish–kebab structure on the bone-binding ability of the composite scaffolds was evaluated by examining the formation of apatite on the surface of the scaffolds. To the best of our knowledge, this is the first report to investigate the effect of the shish–kebab structure on the growth of human cells (MG63, an osteoblast-like cell line) for bone tissue engineering.

Materials and methods

Materials

Poly(ε-caprolactone) (PCL, Capa® 6500, Mn = 50,000) was purchased from Perstorp (London, UK). Chloroform (ACS regent), *N*,*N*-dimethyl formamide (DMF) (ACS regent), nanosize HA, and all analytical grade chemicals for making SBF were purchased from Sigma-Aldrich (Milwaukee, WI, USA). The morphology of the nanosize nHA is shown in Fig. 1, indicating that the size of the nHA particle is smaller than 200 nm.

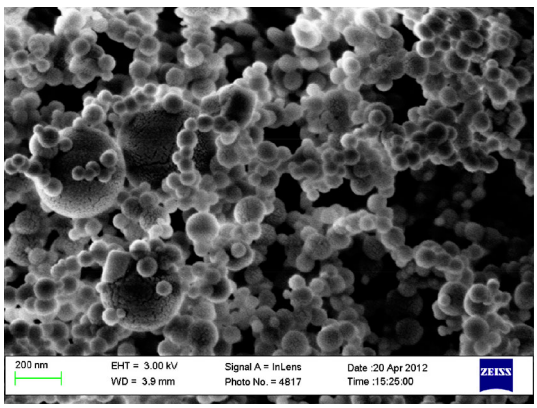

Fig. 1 SEM image of the as-received nanoHA particles

Electrospinning

Electrospinning of PCL nanofibers

PCL pellets were dissolved in a mixture of chloroform and DMF (v/v = 6/4) to form a 14 wt% solution. The solution was loaded into a 6-mL syringe connected by Teflon tubing (PTFE Tubing, 1/32″ ID × 1/16″ OD, Fisher Scientific, USA) to an 18-gage blunt needle (Fisher Scientific, USA). A flow rate of 0.5 mL/h was obtained using a syringe pump (Syringe Pump 11, Harvard Bioscience Company, USA). The applied voltage was 18 kV. Grounded aluminum foil (Fisher Scientific, USA) and round stainless steel washers (inner diameter of 8.33 mm, McMaster-Carr. Co, USA), kept 17 cm away from the needle tip, were used as collectors. In electrospinning, the collectors should be conductive to achieve a uniform fiber structure. Hence, sterilized stainless steel washers were used to collect samples for cell culture because of their non-cytotoxicity.

Electrospinning of PCL/nHA composite nanofibers

HA nanocrystals (10 % wt. of PCL) were suspended in chloroform/DMF at a 6:4 solvent ratio using ultrasonication (Ultrasonic Cleaners, Fisher Scientific, USA). After subjecting to ultrasound for 30 min, the suspension was added to the PCL/chloroform solution and then subjected to ultrasound for another 30 min to form a PCL/nHA 14 wt% suspension. The resulting solution was then used for electrospun nanofiber formation. The same optimized conditions and processing parameters obtained from electrospinning PCL solution were applied to the PCL/nHA suspension to make a better comparison.

Hierarchically decorated nanofibers

A dilute PCL solution was used to form the nanohybrid shish–kebab structure on the surface of the electrospun nanofibers. A detailed procedure can be found in our previous study [21]. Briefly, 0.5 wt% PCL in a mixture of acetic acid and deionized water (acetic acid: deionized water = 77:23 v/v) was prepared. Dilute PCL solution was slowly drop cast on the nanofibrous PCL or PCL/nHA membrane. The volume of the dilute PCL solution used to wet the membrane was adjusted according to membrane surface area. Membranes were then dried in a fume hood to evaporate the solvent.

Preparation of simulated body fluids (2 × SBF)

Simulated body fluid solution (SBF) was prepared using established protocols [22]. Briefly, reagents NaCl, $NaHCO_3$, KCl, $K_2HPO_4{\cdot}3H_2O$, $MaCl_2{\cdot}6H_2O$, 1 mol/L HCl, $CaCl_2$, and Na_2SO_4 were added in sequence, and the pH value of the solution was adjusted to 7.4 at 36.5 °C by adding $(CH_2OH)_3CNH_2$. To accelerate mineralization, ion concentrations in SBF were doubled (2 × SBF). Major ion concentrations in the solution are compared to those in human blood plasma (Table 1).

Biomimetic mineralization in 2 × SBF

Dried mats (1 cm × 1 cm) were incubated in 2 × SBF in 12-well plates at 37 °C. The 2 × SBF solution was refreshed every 3 days during mineralization. Before use, the 2 × SBF solution was stored at 4 °C overnight to allow it to stabilize.

In vitro cell culture

For the cell culture work, MG-63 cell line (Lonza, Allendale, NJ, USA) was plated in 175 cm^2 cell culture flasks at a density of 75,000/cm^2 and cultured in Dulbecco's Modified Eagle's Medium (DMEM) supplemented with 10 % FBS and 1 % antibiotics (10000 IU/mL penicillin, 10000 μg/mL streptomycin, and 25 μg/mL amphotericin B). When cells reached 80 % confluency, they were passaged using 0.05 % trypsin EDTA 1× and counted with a hemocytometer to obtain the cell density.

The scaffolds were first stored in a vacuum oven for 2 days at 45 °C to evaporate the residual solvent, sterilized under UV light for 30 min on both sides, and then soaked in 70 % ethanol for another 30 min. To rehydrate the scaffolds, they were first washed twice with HyPure cell culture grade water and then soaked in phosphate buffered saline (PBS) (South Logan, UT, USA) overnight. In the next day, the scaffolds were washed with PBS two more times and transferred to 24-well tissue culture plates that had been treated with 0.5 mL of 0.5 % poly(2-hydroxyethyl methacrylate) (PolyHEMA, Polysciences, Warrington, PA) to prevent cell adhesion to the plates. Scaffolds seeded with MG-63 cells at a density of 2 × 10^4 cells/cm^2 [23] were cultured in 10 % FBS medium supplemented with 10 mM β-glycerophosphate, 50 μg/mL L-ascorbic acid 2-phosphate, and 100 nM dexamethasone. Culture medium was changed every 3 days.

Characterization

Solution conductivity and viscosity

The conductivities of the solutions prepared for electrospinning were measured using a conductivity instrument (AP85 Portable, Fisher Scientific, USA). The conductivity meter was calibrated to the 0.0–19.9 μS range prior to use.

Table 1 Ion concentrations of simulated body fluid and human blood plasma

Ion	Simulated body fluid SBF (mM)	Concentrated simulated body fluid (2 × SBF)	Human blood plasma (mM)
Na^+	142	284	142
K^+	5	10	5
Mg^{2+}	1.5	3	1.5
Ca^{2+}	2.5	5	2.5
Cl^-	147.8	295.6	103.0
HCO_3^-	4.2	8.4	27
HPO_4^{2-}	1.0	2	1
SO_4^{2-}	0.5	1	0.5

The viscosities of the solutions prepared were tested via a Brookfield rheometer (Brookfield, USA).

Gel permeation chromatography (GPC)

The molecular weight of PCL before and after ultrasonication was measured with a model VE2001 gel permeation chromatographer (GPC) equipped with a 302 tetra detector array. Tetrahydrofunan (THF, HPLC grade, Fisher Scientific) was used as an eluent, and the flow rate was set to 1 mL/min with an injection volume of 100 μL. Calibrations of columns were carried out using a standard polystyrene (PS) solution. All test solutions were prepared at a concentration of 2.5 mg/mL.

Morphological characterization

The morphologies of nHA and electrospun nanofibrous samples were observed by scanning electron microscopy (SEM) (LEO GEMINI 1530) with an accelerating voltage of 3 kV. Energy dispersion X-ray (EDS) analysis was also conducted under SEM to investigate the distribution of nHA particles in the membrane. The calcium (Ca) element was mapped as an indicator of nHA location and concentration. Prior to SEM imaging, samples were sputter coated with gold. SEM images were analyzed with ImageJ Software to measure fiber diameters and obtain NFSK geometric information and pore sizes based on the method reported in the published report [24]. Three SEM images were used to obtain the average values and standard deviation.

Determination of water contact angle (WCA)

Before water contact angle measurement, the prepared scaffolds were rinsed with deionized water three times, put in a fume hood for 3 days, and then stored in a vacuum oven at 45 °C for 48 h until the odor of acid completely disappeared. Surface water contact angles (WCAs) were tested using the sessile drop method at room temperature with a video contact angle instrument (Dataphysics OCA 15). The droplet size was set at 4 μL. Surface contact angle was measured 15 s after dropping the liquid. Three samples for each group were tested and the average value was reported with standard deviation (±SD).

Mechanical properties

The mechanical properties of the prepared scaffolds were investigated following published methods [25]. Electrospun membranes were configured into rectangular shapes with dimensions of 15 × 10 mm^2 (length × width). Tensile tests were performed on an Instron 5565 universal testing machine using a 250 N load cell with a crosshead speed of 5 mm/min. At least four samples were tested for each type of electrospun fibrous membrane. Ultimate tensile strength, Young's modulus, and elongation-at-break were obtained from the stress–strain curves.

Biomineralization behavior characterization

Mineralized membranes after 3 days, 1 week, and 2 weeks were coated with gold and imaged using the previous mentioned SEM. Energy dispersive X-ray spectroscopy (EDS) was used to analyze the mineralized HA elements on the samples after 1 week via the same instrument. A square area was scanned, and elements within that area were quantified.

Cell adhesion and proliferation

To study the cell adhesion and proliferation on different substrates, the cells cultured on the substrates after 12 h, 10 days, and 21 days of culture were initially washed twice with PBS to ensure that the cells collected were not growing in suspension within the poly-HEMA coated plates. TrypLE (Life Technologies) was then used to detach the cells for 5 min at 37 °C. After incubation, the cells were collected and centrifuged at 200 rpm for 5 min. The supernatant was then aspirated, and the cells resuspended

in 600 μL of PBS and filtered prior to analysis. Data were acquired with an Accuri C6 flow cytometer (BD Biosciences).

Alkaline phosphatase quantitative analysis

The ALP activity of cells on scaffolds was tested after 10 days and 14 days culture. Cell lysates for the quantification of double-stranded DNA (dsDNA) were used for analysis of ALP activity. Briefly, cellular scaffolds were collected, washed with 1× Tris-buffered saline (TBS), and incubated in a cell digestion buffer (150 mM Tris base, 0.1 mM $ZnCl_2$, and 0.1 mM $MgCl_2$) for 30 min at 37 °C, and then overnight at 4 °C to lyse cells. The content of the dsDNA in the cell lysates was determined using a Quant-iT™ Pico Green® dsDNA assay kit (Invitrogen) following the manufacturer's instructions. 100 μL of 5 mM SIGMA 104 (Sigma) was added to 100 μL of cell lysate to detect ALP activity by measurement of absorbance wavelength at 410 nm every 3 min for 30 min. The ALP activity of each sample was normalized with the dsDNA amount of the same sample.

Calcium quantification

Scaffolds seeded with the MG-63 cells were harvested after 10 days and 21 days culture to quantify the cellular calcium production. To harvest, scaffolds were rinsed twice with PBS and then transferred to 1.7 mL microcentrifuge tubes. 250 μL of 0.5 M HCl was added to each tube. Tubes were incubated at 4 °C overnight on a shaker. In the next morning, samples were moved to −80 °C until all samples had been obtained. To examine the calcium content, samples were thawed, vortexed, and centrifuged at 500 rpm for 2 min. A StanbioTotal Calcium LiquiColor kit was used to quantify the calcium content following the manufacturer's protocol. Briefly, equal parts of the total calcium color reagent and total calcium base reagent were mixed to form the working reagent and allowed to stand at room temperature for 15 min prior to use. Equal volumes of sample and working reagent were added to wells of a 96-well plate, mixed well, and read at an absorbance of 550 nm.

Cytoskeleton study

Actin staining was conducted on the scaffolds after seeding cells for 2 days to determine the shape and cytoskeleton organization of the cells. After 2 days, cells were stained with a phalloidin conjugate to stain actin and DAPI to stain the nucleus (Life Technologies, Grand Island, NY, USA). Scaffolds were washed twice with PBS, fixed for 5 min in 4 % formaldehyde (Polysciences, Warrington, PA, USA), and washed extensively in PBS. To permeabilize the cells, 0.3 % Triton X-100 (LabChem Inc, Pittsburgh, PA, USA) in PBS was added to the scaffolds for 5 min. Scaffolds were then washed extensively with PBS and blocked for 1 h with 3 % BSA in PBS to prevent nonspecific phalloidin staining. After 1 h, scaffolds were again washed extensively with PBS and then stained with 50 μg/mL of a fluorescent phalloidin conjugate solution in PBS for 40 min at room temperature in the dark. After 40 min, scaffolds were washed 4 times with PBS. A drop of 4′,6-diamidino-2-phenylindole (DAPI) stain was added as a mounting solution. Scaffolds were imaged using a Nikon Eclipse E600 microscope with a Nikon Y-FL EPI fluorescence unit (Chiyoda, Tokyo).

Statistical analysis

All of the quantitative results were expressed as mean ± standard deviation (SD). Statistical analyses were carried out by means of a one-way analysis of variance (ANOVA). A p value less than 0.05 was considered statistically significant.

Results and discussion

Morphology of the electrospun and hierarchically decorated nanofibers

The morphology of electrospun PCL, PCL/nHA composite nanofibers, PCL NFSK, and PCL/nHA NFSK are shown in Fig. 2. Undecorated PCL nanofibers were smooth and bead-less. However, the diameters of PCL fibers ranged from less than 100 nm to over 1,000 nm. Non-uniformity of the fibers might be a result of the poor conductivity of the electrospun solution [26]. HA-incorporated PCL fibers were also free of beads, and the average diameter of the PCL/nHA fibers was 296 ± 121 nm, similar to the 294 ± 106 nm found for undecorated PCL fibers [27]. However, PCL/nHA contained a larger percentage of thinner fibers compared to pure PCL fibers, and the fiber distribution was broader (shown in Fig. 3).

To understand the effect of nHA on the morphology of electrospun nanofibers, the conductivity and viscosity of the PCL/nHA composite solution after ultrasonication for 30 min were immediately measured, and it was found that the conductivity increased from 0.6 μS/cm for the PCL solution to 1.7 μS/cm for the PCL/nHA composite solution [28]. However, the viscosity of the composite solution decreased from 0.058 Pa s for the PCL solution to 0.055 Pa s. Although it has been reported that the interaction between PCL and nHA could result in an increase of the viscosity of the electrospun solution [29], due to the ultrasonication used in this study to better disperse HA in

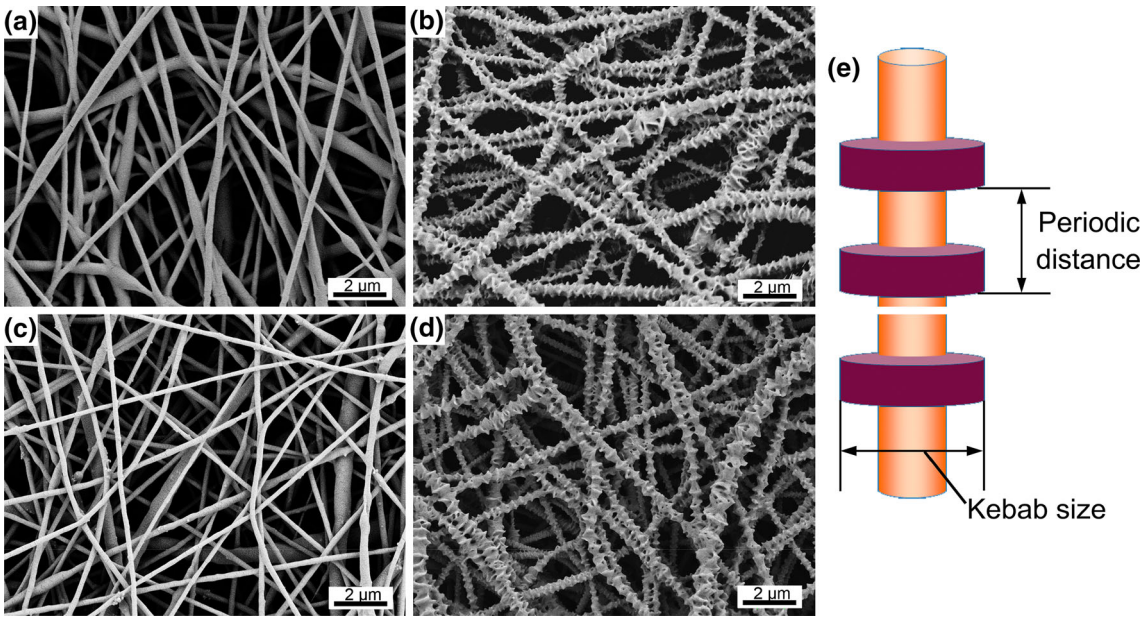

Fig. 2 SEM images of **a** PCL **b** PCL NFSK, **c** PCL/nHA, and **d** PCL/nHA NFSK scaffolds and **e** schematic representation of the prepared shish–kebab structure

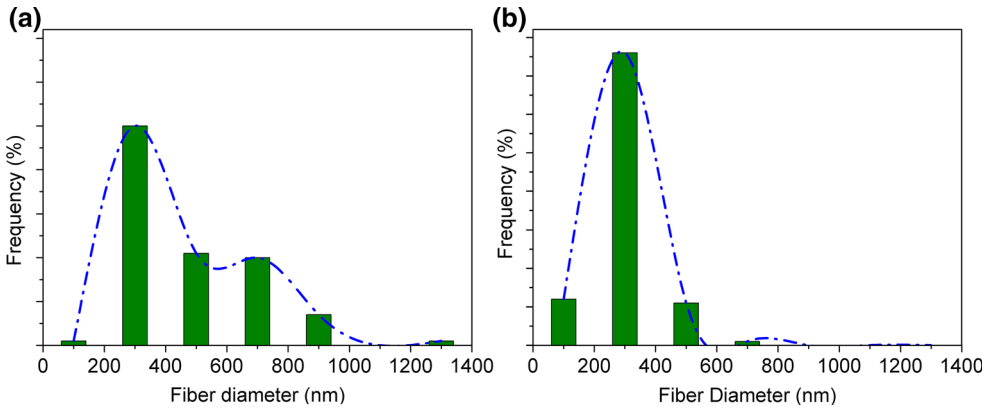

Fig. 3 The fiber diameter distribution of **a** PCL and **b** PCL/nHA electrospun scaffolds

the electrospun solution, the molecular weight of PCL decreased slightly (the Mw of PCL decreased from 158 kDa before ultrasonication to 132 kDa after ultrasonication), which induced a decrease in the viscosity of the composite solution. During electrospinning, an increase in conductivity causes a higher electrical force, hence resulting in thinner fibers. A lower viscosity of the polymer solution also enables the formation of thinner fibers.

A representative SEM image of the PCL NFSK structure is shown in Fig. 2b. PCL nanofibers were decorated with PCL crystal lamellas orthogonal to the fiber axis. 2-D "disk-like" PCL lamellae crystals periodically grew onto the nanofibers, resembling the shish–kebab structure. Morphologically, the central nanofiber is the "shish" while the induced crystals on the surface are "kebabs." The dimensional features of our shish–kebab structures are defined in a schematic image (Fig. 2e). Periodic distance between the kebabs was 362 ± 89 nm, and crystal lateral size was 488 ± 92 nm, indicating successful formation of a 3-D nanostructure on top of the smooth PCL nanofibers. The detailed mechanism has been reported in our previous study [21]. When shish material was changed into PCL/nHA, properly formed NFSKs were also observed (Fig. 2d). Kebab size of PCL/nHA NFSK was 427 ± 62 nm, and the periodic distance of the kebabs were 410 ± 100 nm, demonstrating that introduction of nano-sized nHA affected both the periodic distance and the kebab size of the shish–kebab structures. Compared with original PCL and PCL/nHA nanofibers, it is interesting to note that PCL lamellae crystal growth between nanofibers created a "tie" that bonded the fibers together (Fig. 4c, d). In the PCL/nHA NFSK, more "tie" structures occurred.

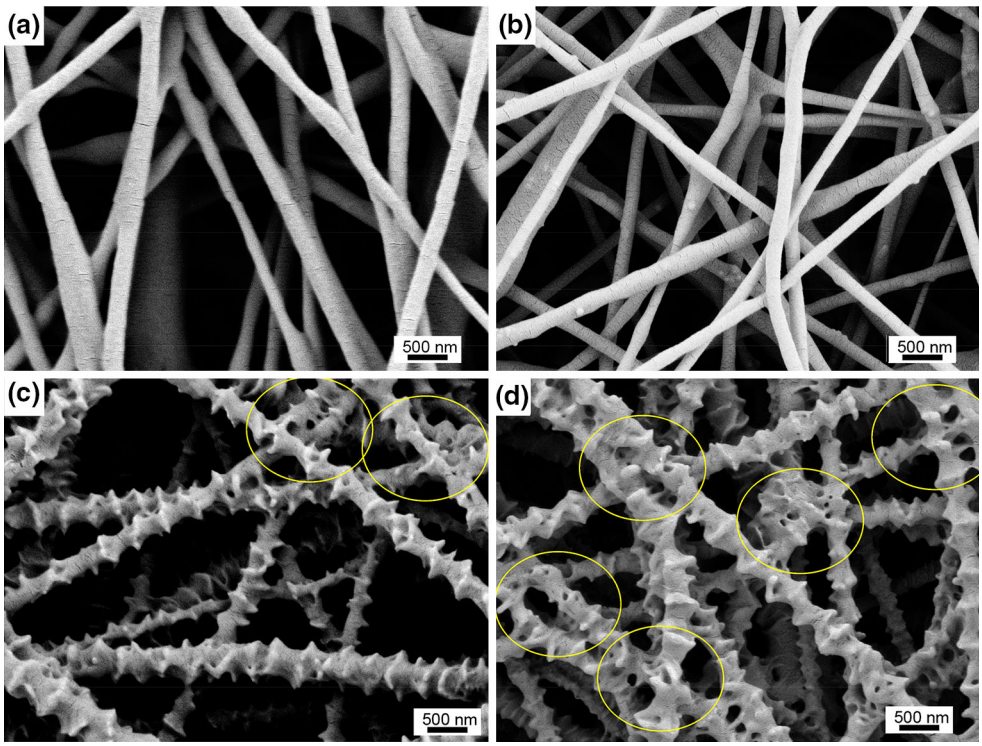

Fig. 4 SEM images of **a** PCL, **b** PCL/nHA, **c** PCL NFSK, and **d** PCL/nHA NFSK at high magnification, and cycles indicates the "ties" that bond fibers together

This is possibly caused by altered behavior due to the presence of exposed nanosized nHA particles. Exposed nanosized nHA particles in the joint of the fibers acted as heterogeneous agents to attract more aggregated PCL molecules. These aggregated molecules formed chains around HA particles to form more "ties." As more "ties" were formed, fibers became woven into interlocking mats which likely had greater structurally stability and strength than unwoven nanofibers.

Water contact angle

The surface wettability of different scaffolds is shown in Fig. 5a–d. WCAs for undecorated PCL and PCL/nHA composite scaffolds were 131.6 ± 0.6° and 136.3 ± 0.2°, respectively. This indicated the hydrophobic property of PCL. For nanofibers with NFSK, the water contact angle was smaller, especially for PCL/nHA NFSK which decreased to 117.5 ± 1.1°. This change in material properties might be attributed to the increased openness of the NFSK structure due to spaces created by the kebabs which kept the fibers apart [30]. The pore size (shown in Table 1) of the shish–kebab structured scaffolds increased, especially for PCL/nHA NFSK which increased from 1.5 to 2.2 μm as compared to its counterparts. This increased pore size inside the scaffolds could have resulted in easier water infiltration, thus, leading to a smaller water contact angle.

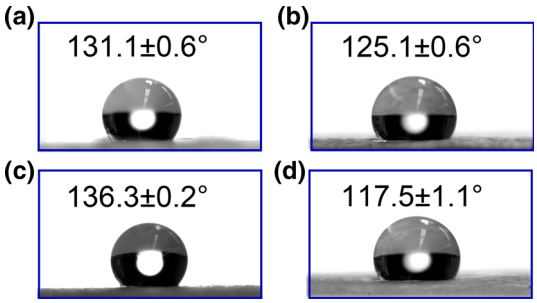

Fig. 5 Water contact angle results of **a** PCL, **b** PCL NFSK, **c** PCL/nHA, and **d** PCL/nHA NFSK scaffolds

Mechanical properties

The mechanical properties of electrospun nanofibers and their NFSK counterparts were characterized by tensile tests. For electrospun membranes, it is difficult to prepare standard specimens for tensile tests. Therefore, we cut them into the same shapes and dimensions for better comparison among the specimens based on published protocols. Young's modulus, tensile strength, and elongation-at-break of the samples are shown in Fig. 6. The PCL/nHA scaffolds show higher moduli than naked PCL fibers (Table 2), indicating that nHA had a reinforcing effect on the polymer matrix [28]. However, due to the brittle nature of nHA, elongation of the PCL/nHA composite scaffolds was slightly decreased [31]. It was surprising to find that,

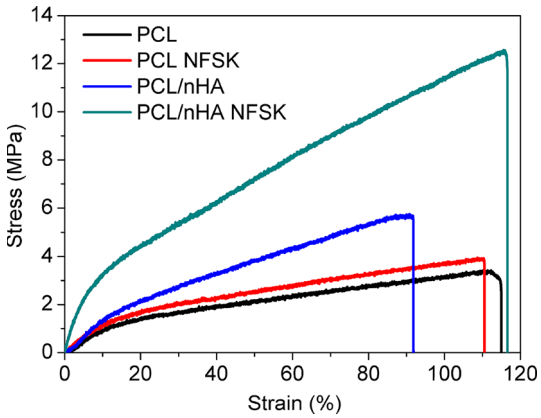

Fig. 6 Representative stress–strain curves of the tested scaffolds

after decorating the electrospun fibers, the mechanical properties of the scaffolds were greatly enhanced, especially for PCL/nHA NFSK. Increased mechanical properties are likely caused by PCL crystal lamella on the surface of the fibers, especially in the joints between the fibers, since it is believed that the crystal lamella were better for load transfer during testing. Similar results have been reported in poly(L-lactide)/carbon nanotube (PLLA/CNT) nanocomposite fibers with a shish–kebab structure, in which the poly(L-lactide) lamella acted as kebabs while the carbon nanotube fibers acted as the shish. With the decoration of PLLA on the CNT surface as a binder, the tensile strength of the nanocomposite fibers improved [32]. Therefore, in this study, due to the created PCL lamella on the surface of the nanofibers, the mechanical properties of the nanofibers were enhanced. Moreover, on the surface of the PCL/nHA NFSK nanofibers, more "ties" (which is the overgrowth of PCL crystal lamella) were created than on the PCL NFSK, resulting in a more significant enhancement in mechanical properties.

Biomimetic mineralization

It has been reported that when bioactive materials are implanted in the body, they spontaneously bond to bone via an apatite layer deposited on their surface [33]. Researchers have been using a SBF to test this phenomenon in vitro due to the difficulty of in vivo testing [34]. 2 × SBF was used as the mineralization media in our study to examine biomimetic mineralization of the scaffolds [35]. As shown in Fig. 7, after 7 days exposure to SBF, some minerals start to form on the surface of the membrane. The apatite layer only deposited on top of the PCL and PCL/NFSK scaffolds. This ineffective coating was ascribed to the relatively inert surface of PCL, which lacks the ability to bond to calcium phosphate [36]. However, on the surface of the PCL/nHA mat, more homogeneous apatite crystals were formed. This was because the induced HA led to an enrichment of Ca^{2+} in the SBF solution, resulting in local super-saturation and crystal nucleation [37]. On the other hand, a layer of randomly oriented plate crystals formed along the fibers, and the shish–kebab structure was completely covered on the PCL/nHA NFSK mat, indicating an overgrowth of minerals. The architecture of the electrospun mats, especially the greater pore size and interfiber spacing over the PCL/nHA, resulted in an increased dissolution of ions, and subsequently, a higher deposition of apatite [14].

To determine the composition and structure of the mineral phase grown on the samples, EDS mapping was performed under SEM (Fig. 8). By using the intensity of the carbon element as a reference, it was determined that the intensities of calcium and phosphorus in PCL/nHA NFSK were higher than other groups. This indicated that there was more apatite deposited on the surface of PCL/nHA NFSK. In addition, evolution of the morphology of apatite deposited on PCL NFSK and PCL/nHA NFSK for 3 days, 7 days, and 14 days was observed at high magnification (cf. Figure 9). Accumulating apatite nucleated into a cauliflower shape in 2 × SBF on PCL NFSK and PCL/nHA NFSK after 3 days. The cauliflower "flower petals" became larger after immersion in SBF for 7 days. After submersion in SBF for 14 days, the cauliflower shape evolved into denser apatite flakes and worm-like shapes. This change in nanostructure as apatite was deposited on the samples was also observed in a previous study [38].

Cell adhesion and proliferation

Cellular adhesion and proliferation were examined on day 0, day 10, and day 21 using a Flow Cytometer. The PCL/nHA NFSK scaffold supported the greatest cell adhesion, closely followed by PCL/nHA and PCL NFSK while the smooth PCL scaffold supported the lowest cell adhesion (shown in day 0 in Fig. 10). Previous research indicated that PCL/nHA composite scaffolds enhanced cell adhesion

Table 2 Mechanical properties of PCL and PCL/nHA nanofibers with and without NFSK

Sample	Young's modulus (MPa)	Tensile strength (MPa)	Elongation (%)	Pore size (μm)
PCL	10.5 ± 0.7	3.2 ± 0.1	108.6 ± 3.8	1.8 ± 0.9
PCL NFSK	11.2 ± 0.8	3.5 ± 0.4	105.5 ± 2.2	2.1 ± 0.7
PCL/nHA	16.6 ± 2.1	6.5 ± 0.7	82.2 ± 12.1	1.5 ± 0.6
PCL/nHA NFSK	30.7 ± 1.2	12.1 ± 0.6	115.5 ± 1.5	2.2 ± 1.1

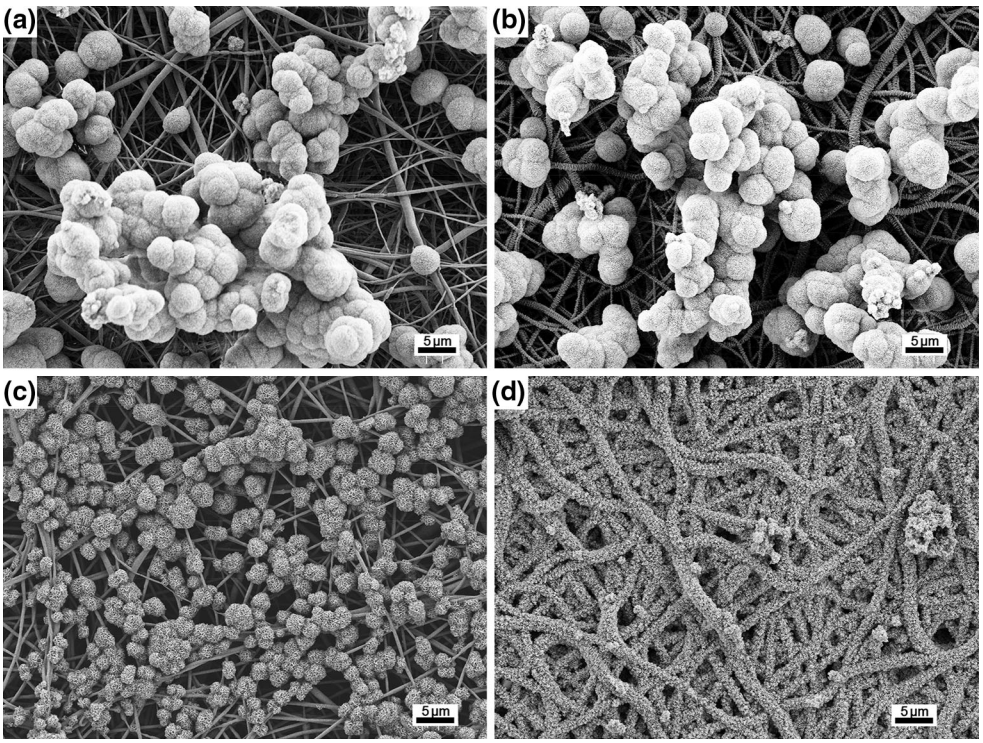

Fig. 7 SEM images of **a** PCL, **b** PCL NFSK, **c** PCL/nHA, and **d** PCL/nHA NFSK after mineralization for 7 days

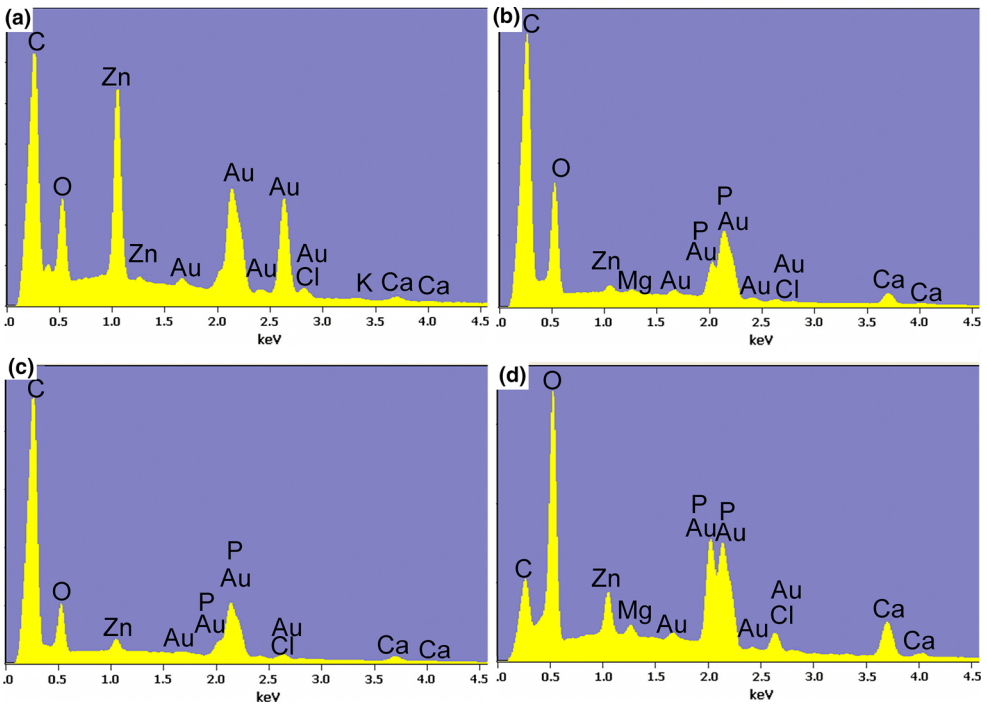

Fig. 8 EDS patterns of **a** PCL, **b** PCL NFSK, **c** PCL/nHA, and **d** PCL/nHA NFSK after immersing in 2 × SBF for 7 days

[39] and cell proliferation [40] compared to PCL scaffolds due to the biologically relevant binding sites on the surface of nHA. Our data for regular PCL and PCL/nHA scaffolds were consistent with these findings (shown in Fig. 10). However, the scaffolds with a shish–kebab structure were more favorable for cell adhesion compared to the smooth

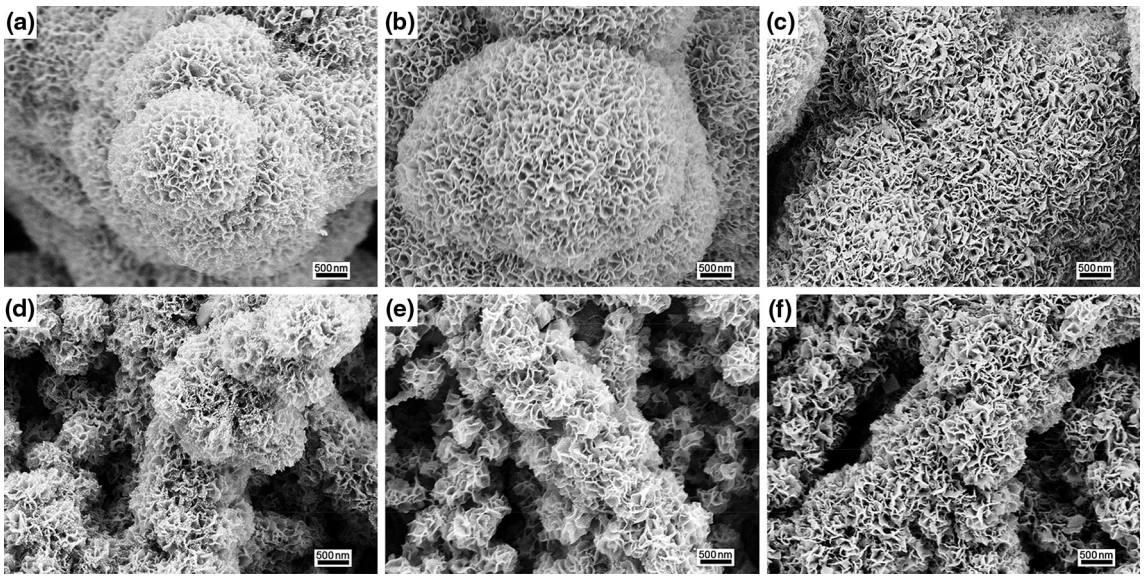

Fig. 9 The morphology evolution of the apatite layer formed on **a** PCL/NFSK for 3 days, **b** PCL/NFSK for 1 week, **c** PCL/NFSK for 2 weeks, **d** PCL/nHA NFSK for 3 days, **e** PCL/nHA for 1 week, and **f** PCL/nHA NFSK for 2 weeks

scaffolds, demonstrating that surface topography affects cell attachment on the scaffolds.

An increase in surface roughness has previously been linked to increased cell proliferation [41]. In consistent with previous report, PCL NFSK scaffolds also enhanced proliferation compared to smooth PCL scaffolds after 10 days culture. Furthermore, cell number was also higher on PCL/nHA NFSK than that on PCL/nHA scaffold, probably due to the higher cell attachment initially. After day 21, PCL/nHA NFSK showed the highest cell population among the scaffolds. PCL/nHA had the next highest cell proliferation, followed by PCL NFSK, with the smooth PCL scaffolds still showing the lowest cell proliferation. Cell proliferation for scaffolds containing nHA appeared to not only depend on the biological binding sites but also depend on nanotopography of the scaffolds [10]. However, our data also indicated that for the PCL/nHA scaffolds, the cell proliferation rates

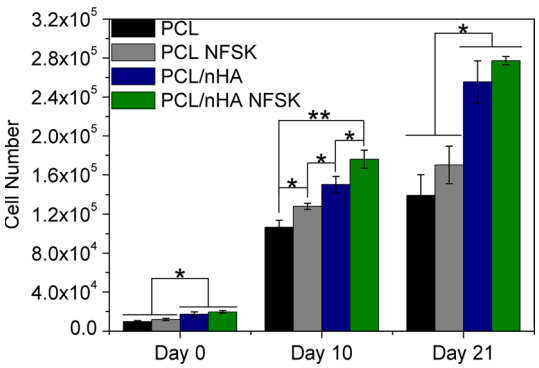

Fig. 10 Cell adhesion and proliferation results of MG63 cultured on PCL, PCL NFSK, PCL/nHA, and PCL/nHA NFSK scaffolds at day 0, day 10, and day 21 ($*p < 0.05$, $**p < 0.01$)

on the NFSK scaffolds were not significant, which may have been due to the binding cites on the HA particles being buried by the shish–kebab structure.

Osteoblast activity

Due to the accumulation of apatite on the PCL/nHA NFSK scaffolds in the presence of SBF, it was hypothesized that nHA-containing scaffolds with a shish–kebab structure would enhance mineralization and support osteoblast activity. Quantitative calcium and ALP assays were performed to examine osteoblast-induced matrix mineralization. It is known that ALP plays an important role in mineralization [42] and is expected to be present when osteoblast activity occurs. On day 10 and day 21, ALP activity was the highest in cells cultured on PCL/nHA NFSK and smooth PCL/nHA scaffolds, indicating enhanced osteoblast mineralization activity on scaffolds containing nHA (Fig. 11). This coincides with previous research, which found that HA composite scaffolds increased ALP activity and matrix mineralization [42]. On PCL NFSK, ALP activity was also higher than on smooth fibers, which demonstrates that the rough surface enhanced osteoblast activity as well. For the calcium activity test, the PCL/nHA and PCL/nHA NFSK scaffolds had HA particles that caused the significantly higher calcium activity, and the contributions from the cells might not have been obvious. Therefore, the results were not given here.

Cell morphology

To gain further understanding of the cellular response to shish–kebab textured scaffolds, MG-63 cells were seeded

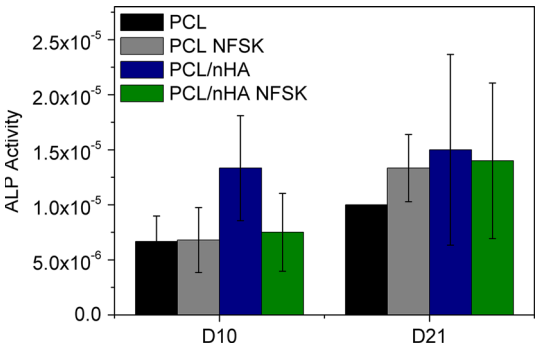

Fig. 11 Quantitative ALP activity results of MG63 cultured on PCL, PCL NFSK, PCL/nHA, and PCL/nHA NFSK at day 10 and day 21

onto the scaffolds and stained with phalloidin after 48 h to examine cell morphology. It was found that cells on PCL/nHA and PCL/nHA NFSK scaffolds presented spindle shape, especially on PCL/nHA NFSK scaffolds, cells showed obvious extended pseudopodia of filament, indicating that there was good interaction between cells and scaffolds. While cells on PCL scaffolds were more rounded (Fig. 12), in contrast, cells were more stretched on PCL NFSK scaffolds. The difference of surface roughness between the smooth and rugged scaffolds clearly contributed to the morphological differences. It is likely that cell adhesion was more limited on PCL scaffolds because of the lack of cell binding sites on PCL fibers and cell adhesions were weak. Therefore, cell adhesions were restricted to limited areas, resulting in a rounded morphology and lower cytoskeletal tension. On the other hand, PCL NFSK had higher surface area ratio due to the special structure which might allow that the scaffolds absorb more vitronectin and fibronectin molecules for cell adhesion [43]. Also, it has been previously reported that the loaded HA was beneficial for cell growth due to the enrichment in integrin binding sites of HA. Hence, cells on the PCL/nHA and PCL/nHA NFSK nanofiber scaffolds were able to bind more freely and follow previously observed patterns [44, 45] where the cells stretched out along the nanofiber due to the abundance of binding sites for cell adhesion on the scaffolds. Moreover, cells showed a more spread morphology on PCL/nHA NFSK than on PCL/nHA, indicating that the advantage of the enhanced surface roughness of PCL/nHA NFSK was predominant in regulating cell morphology.

Cell morphology differences have also been linked to altered cell behavior [46, 47]. It is likely that alterations in MG-63 activity can be linked to changes in cell morphology due to cell interactions with the smooth and shish–kebab scaffolds. Greater cytoskeletal tension has been linked to enhanced mineralization [47]. Our quantitative ALP was consistent with these findings. Cells that exhibited an elongated morphology and greater cytoskeletal tension on PCL/nHA and PCL/nHA NFSK scaffolds exhibited higher ALP activity compared to undecorated PCL scaffolds.

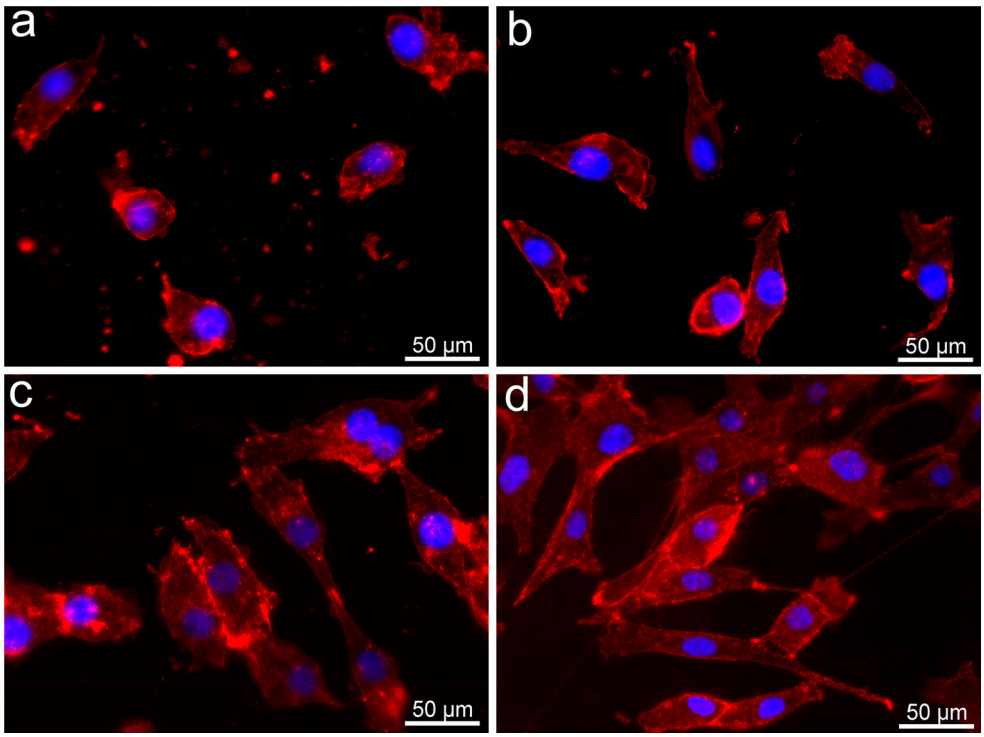

Fig. 12 Cytoskeleton study of MG63 cultured on **a** PCL, **b** PCL NFSK, **c** PCL/nHA, and **d** PCL/nHA NFSK scaffolds (The *red color* demonstrates the actin bundles in the cell membrane and *blue colors* represents the cell nuclei) (Color figure online)

Conclusions

PCL NFSK and PCL/nHA NFSK structures, which are similar in nanotopography to collagen fibrils in bone, were created by electrospinning nanofibers and inducing periodic PCL crystallization on the nanofiber surface. The introduction of nHA in the shish not only changed the microstructure of the shish–kebab fibers but also the macroscopic behavior of scaffolds with regard to the surface wettability and mechanical properties. PCL/nHA NFSK fibers were hydrophilic while undecorated PCL and PCL/nHA were hydrophobic. The shish–kebab structure also resulted in enhanced mechanical properties. Further examination of scaffolds revealed that, in the presence of SBF, a bone-like apatite layer formed on the PCL/nHA NFSK not only on the exterior but also in the interior. The accumulation of minerals on the PCL/nHA NFSK scaffolds encouraged further investigation of the usefulness of the shish–kebab structure in the presence of cells. In the MG-63 osteosarcoma cell culture tests, it was found that the addition of nHA enhanced cell proliferation and functionality. Moreover, PCL/nHA NFSK scaffolds with a shish–kebab structure demonstrated enhanced cell mineralization. Undecorated PCL/nHA scaffolds also yielded enhanced mineralization compared to other scaffolds without shish–kebab structure due to the biological binding sites of nHA on the surface. Given these results, it is likely that the addition of a shish–kebab structure and HA would be useful in applications where matrix mineralization were desirable in bone tissue engineering.

Acknowledgements The authors would like to acknowledge the support of the Wisconsin Institute for Discovery (WID), the China Scholarship Council, the financial support of the National Nature Science Foundation of China (No. 51073061, No. 21174044), the Guangdong Nature Science Foundation (No. S2013020013855, No. 9151064101000066), and the National Basic Research Development Program 973 (No. 2012CB025902) in China.

References

1. Weiner S, Wagner HD (1998) The material bone: structure mechanical function relations. Annu Rev Mater Sci 28:271–298
2. Weiner S, Traub W (1986) Organization of hydroxyapatite crystals within collagen fibrils. FEBS Lett 206:262–266
3. Fratzl P, Weinkamer R (2007) Nature's hierarchical materials. Prog Mater Sci 52:1263–1334
4. Azami M, Moosavifar MJ, Baheiraei N, Moztarzadeh F, Ai J (2012) Preparation of a biomimetic nanocomposite scaffold for bone tissue engineering via mineralization of gelatin hydrogel and study of mineral transformation in simulated body fluid. J Biomed Mater Res A 100A:1347–1355
5. Chen JL, Chu B, Hsiao BS (2006) Mineralization of hydroxyapatite in electrospun nanofibrous poly(L-lactic acid) scaffolds. J Biomed Mater Res A 79A:307–317
6. Nguyen TH, Bao TQ, Park I, Lee BT (2013) A novel fibrous scaffold composed of electrospun porous poly(epsilon-caprolactone) fibers for bone tissue engineering. J Biomater Appl 28: 514–528
7. Jegal SH, Park JH, Kim JH et al (2011) Functional composite nanofibers of poly(lactide-co-caprolactone) containing gelatin-apatite bone mimetic precipitate for bone regeneration. Acta Biomater 7:1609–1617
8. Phipps MC, Clem WC, Grunda JM, Dines GA, Bellis SL (2012) Increasing the pore sizes of bone-mimetic electrospun scaffolds comprised of polycaprolactone, collagen I and hydroxyapatite to enhance cell infiltration. Biomaterials 33:524–534
9. Xie JW, Li XR, Lipner J et al (2010) "Aligned-to-random" nanofiber scaffolds for mimicking the structure of the tendon-to-bone insertion site. Nanoscale 2:923–926
10. Li WJ, Laurencin CT, Caterson EJ, Tuan RS, Ko FK (2002) Electrospun nanofibrous structure: a novel scaffold for tissue engineering. J Biomed Mater Res 60:613–621
11. Wutticharoenmongkol P, Sanchavanakit N, Pavasant P, Supaphol P (2006) Preparation and characterization of novel bone scaffolds based on electrospun polycaprolactone fibers filled with nanoparticles. Macromol Biosci 6:70–77
12. Venugopal J, Low S, Choon AT, Kumar AB, Ramakrishna S (2008) Electrospun-modified nanofibrous scaffolds for the mineralization of osteoblast cells. J Biomed Mater Res A 85A: 408–417
13. Puppi D, Piras AM, Chiellini F et al (2011) Optimized electro- and wet-spinning techniques for the production of polymeric fibrous scaffolds loaded with bisphosphonate and hydroxyapatite. J Tissue Eng Regen Med 5:253–263
14. Patlolla A, Arinzeh TL (2014) Evaluating apatite formation and osteogenic activity of electrospun composites for bone tissue engineering. Biotechnol Bioeng 111:1000–1017
15. Fang M, Goldstein EL, Matich EK, Orr BG, Holl MMB (2013) Type I collagen self-assembly: the roles of substrate and concentration. Langmuir 29:2330–2338
16. Vetrone F, Variola F, de Oliveira PT et al (2009) Nanoscale oxidative patterning of metallic surfaces to modulate cell activity and fate. Nano Lett 9:659–665
17. Binsberg F (1966) Orientation-induced nucleation in polymer crystallization. Nature 211:516–517
18. Pennings AJ, Kiel AM (1965) Fractionation of Polymers by Crystallization from Solution. 3. On Morphology of Fibrillar Polyethylene Crystals Grown in Solution. Kolloid Z Z Polym 205:160–162
19. Li LY, Li CY, Ni CY (2006) Polymer crystallization-driven, periodic patterning on carbon nanotubes. J Am Chem Soc 128:1692–1699
20. Chen X, Wang WD, Cheng S, Dong B, Li CY (2013) Mimicking bone nanostructure by combining block copolymer self-assembly and 1D crystal nucleation. ACS Nano 7:8251–8257
21. Wang XF, Salick MR, Wang XD et al (2013) Poly(epsilon-caprolactone) nanofibers with a self-induced nanohybrid shish-kebab structure mimicking collagen fibrils. Biomacromolecules 14:3557–3569
22. Kokubo T, Takadama H (2006) How useful is SBF in predicting in vivo bone bioactivity? Biomaterials 27:2907–2915
23. Peng F, Yu XH, Wei M (2011) In vitro cell performance on hydroxyapatite particles/poly(L-lactic acid) nanofibrous scaffolds with an excellent particle along nanofiber orientation. Acta Biomater 7:2585–2592
24. Rnjak-Kovacina J, Wise SG, Li Z et al (2011) Tailoring the porosity and pore size of electrospun synthetic human elastin scaffolds for dermal tissue engineering. Biomaterials 32:6729–6736

25. Croisier F, Duwez AS, Jerome C et al (2012) Mechanical testing of electrospun PCL fibers. Acta Biomater 8:218–224
26. Pirzada T, Arvidson SA, Saquing CD, Shah SS, Khan SA (2012) Hybrid silica-PVA nanofibers via sol-gel electrospinning. Langmuir 28:5834–5844
27. Zargarian SS, Haddadi-Asl V (2010) A nanofibrous composite scaffold of PCL/hydroxyapatite-chitosan/PVA prepared by electrospinning. Iran Polym J 19:457–468
28. Thomas V, Jagani S, Johnson K et al (2006) Electrospun bioactive nanocomposite scaffolds of polycaprolactone and nanohydroxyapatite for bone tissue engineering. J Nanosci Nanotechnol 6:487–493
29. Liao GY, Jiang SB, Xia H, Jiang KF (2012) Preparation and characterization of aligned PLLA/PCL/HA composite fibrous membranes. J Macromol Sci A 49:946–951
30. Wang BB, Li B, Xiong J, Li CY (2008) Hierarchically ordered polymer nanofibers via electrospinning and controlled polymer crystallization. Macromolecules 41:9516–9521
31. Thomas V, Dean DR, Jose MV, Mathew B, Chowdhury S, Vohra YK (2007) Nanostructured biocomposite scaffolds based on collagen coelectrospun with nanohydroxyapatite. Biomacromolecules 8:631–637
32. Ning NY, Zhang W, Zhao YS, Luo F, Fu Q (2012) Nanohybrid shish kebab structure and its effect on mechanical properties in poly(L-lactide)/carbon nanotube nanocomposite fibers. Polym Int 61:1634–1639
33. Hench LL, Wilson J (1993) An introduction to bioceramics. World Scientific, London
34. Yu SC, Hariram KP, Kumar R, Cheang P, Aik KK (2005) In vitro apatite formation and its growth kinetics on hydroxyapatite/polyetheretherketone biocomposites. Biomaterials 26:2343–2352
35. Rodriguez K, Renneckar S, Gatenholm P (2011) Biomimetic calcium phosphate crystal mineralization on electrospun cellulose-based scaffolds. Acs Appl Mater Interfaces 3:681–689
36. Yang F, Wolke JGC, Jansen JA (2008) Biomimetic calcium phosphate coating on electrospun poly (epsilon-caprolactone) scaffolds for bone tissue engineering. Chem Eng J 137:154–161
37. Li MM, Liu WW, Sun JS et al (2013) Culturing primary human osteoblasts on electrospun poly(lactic-co-glycolic acid) and poly(lactic-co-glycolic acid)/nanohydroxyapatite scaffolds for bone tissue engineering. Acs Appl Mater Interfaces 5:5921–5926
38. Mi HY, Jing X, Salick MR, Cordie TM, Peng XF, Turng LS (2014) Morphology, mechanical properties, and mineralization of rigid thermoplastic polyurethane/hydroxyapatite scaffolds for bone tissue applications: effects of fabrication approaches and hydroxyapatite size. J Mater Sci 49:2324–2337. doi:10.1007/s10853-013-7931-3
39. Shor L, Guceri S, Wen XJ, Gandhi M, Sun W (2007) Fabrication of three-dimensional polycaprolactone/hydroxyapatite tissue scaffolds and osteoblast-scaffold interactions in vitro. Biomaterials 28:5291–5297
40. Lee HJ, Kim SE, Choi HW, Kim CW, Kim KJ, Lee SC (2007) The effect of surface-modified nano-hydroxyapatite on biocompatibility of poly(epsilon-caprolactone)/hydroxyapatite nanocomposites. Eur Polym J 43:1602–1608
41. Deligianni DD, Katsala ND, Koutsoukos PG, Missirlis YF (2001) Effect of surface roughness of hydroxyapatite on human bone marrow cell adhesion, proliferation, differentiation and detachment strength. Biomaterials 22:87–96
42. Golub EE, Harrison G, Taylor AG, Camper S, Shapiro IM (1992) The role of alkaline-phosphatase in cartilage mineralization. Bone Miner 17:273–278
43. Woo KM, Chen VJ, Ma PX (2003) Nano-fibrous scaffolding architecture selectively enhances protein adsorption contributing to cell attachment. J Biomed Mater Res A 67A:531–537
44. Shi LY, Aid R, Le Visage C, Chew SY (2012) Biomimicking polysaccharide nanofibers promote vascular phenotypes: a potential application for vascular tissue engineering. Macromol Biosci 12:395–401
45. Jiang X, Cao HQ, Shi LY, Ng SY, Stanton LW, Chew SY (2012) Nanofiber topography and sustained biochemical signaling enhance human mesenchymal stem cell neural commitment. Acta Biomater 8:1290–1302
46. Kilian KA, Bugarija B, Lahn BT, Mrksich M (2010) Geometric cues for directing the differentiation of mesenchymal stem cells. Proc Natl Acad Sci USA 107:4872–4877
47. McBeath R, Pirone DM, Nelson CM, Bhadriraju K, Chen CS (2004) Cell shape, cytoskeletal tension, and RhoA regulate stem cell lineage commitment. Dev Cell 6:483–495